



ISSN: 0067-2904

Prediction of the Future Temperature of Baghdad City by Land Surface Temperature (LST) Dynamics Using the BiLSTM Deep Learning Model

Hind S. Harba¹, Eman S. Harba², Inas Ali Abdulmunem^{3*}, Yaseen K. Al-Timimi¹

¹ Department of Atmospheric Sciences, College of Science, University of Mustansiriyah, Baghdad, Iraq

² Avicenna Unit for E-Learning, College of Arts, University of Baghdad, Baghdad, Iraq

^{3*} Department of Computer Science, College of Science University of Baghdad, Baghdad, Iraq

Received: 13/9/2023

Accepted: 31/3/2024

Published: 30/3/2025

Abstract

In recent years, land surface temperature (LST) has become an increasing concern because of the rise in urban temperatures and the accompanying microclimatic warming. The utilization of artificial intelligence models to predict variations in LST is highly beneficial for assessing and forecasting the dynamic climatic changes occurring worldwide. However, the prediction of LST is a difficult task because slight errors in its short-term forecasts can accumulate to become significant errors over longer periods of time. In this paper, a hybrid model that utilizes a bi-directional long short-term memory (BiLSTM) framework is presented for improving the accuracy of long-term LST prediction. The goal is to forecast the future patterns of LST and their possible effects on the urban microclimate of Baghdad city. A high-resolution land cover and land use map for Baghdad City, as well as data collected from satellite photos, were used in this work to construct a surface temperature forecast model. Based on the data analysis, Baghdad experienced the greatest temperature rises from 2001 to 2018, where a fast staggering in LST occurred at $>35^{\circ}\text{C}$ in 2018 due to the net change in the Baghdad area, which was 12.8%. The prediction results show that the proposed BiLSTM model can significantly increase the accuracy of long-range weather forecasts for Baghdad. The results show that the mean-squared error of 0.53 and the correlation coefficient of 0.84 between the predicted and actual LST indicate good accuracy. Hence, the proposed model can be used to estimate future LSTs in Baghdad with low error.

Keywords: geographic information system, bi-directional long short-term memory, convolution neural network, land surface temperature, LST, GIS, deep learning.

التنبؤ بدرجة الحرارة المستقبلية لمدينة بغداد من خلال ديناميكيات درجة حرارة سطح الأرض (LST)

باستعمال نموذج التعلم العميق BiLSTM

هند سليم حربيه¹، ايمان سليم حربيه²، ايناس علي عبدالمنعم^{3*}، ياسين التميمي¹

¹ قسم علم الجو، كلية العلوم، الجامعة المستنصرية، بغداد، العراق

² وحدة ابن سينا للتعليم الالكتروني، كلية الآداب، جامعة بغداد، بغداد، العراق

^{3*} قسم علوم الحاسوب، كلية العلوم، جامعة بغداد، بغداد، العراق

*Email: inas.ali@uobaghdad.edu.iq

الخلاصة

في السنوات الأخيرة، أصبحت درجة حرارة سطح الأرض (LST) مصدر قلق متزايد، بسبب ارتفاع درجات الحرارة في المناطق الحضرية وما يصاحب ذلك من ارتفاع درجة حرارة المناخ المحلي. يعد استعمال نماذج الذكاء الاصطناعي للتنبؤ بالتغيرات في LST مفيداً للغاية لتقييم التغيرات المناخية الديناميكية التي تحدث في جميع أنحاء العالم والتنبؤ بها. ومع ذلك، فإن التنبؤ بـ LST مهمة صعبة لأن الأخطاء الطفيفة في تنبؤاتها قصيرة المدى يمكن أن تتراكم لتصبح أخطاء كبيرة على فترات زمنية أطول. في هذا البحث، تم تقديم نموذج هجين يستعمل إطار الذاكرة طويلة المدى ثنائية الاتجاه (BiLSTM) لتحسين دقة تنبؤ LST طويل المدى. الهدف هو التنبؤ بالأنماط المستقبلية لـ LST وتأثيراتها المحتملة على المناخ الحضري لمدينة بغداد. تم استعمال خريطة عالية الدقة للغطاء الأرضي واستعمال الأراضي لمدينة بغداد، بالإضافة إلى البيانات التي تم جمعها من صور الأقمار الصناعية، في هذا العمل لبناء نموذج للتنبؤ بدرجة حرارة السطح. بناءً على تحليل البيانات، شهدت بغداد أكبر ارتفاع في درجات الحرارة من عام 2001 إلى عام 2018، حيث حدث ارتفاع مذهل في LST عند أكثر من 35 درجة مئوية في عام 2018 بسبب التغير الصافي في منطقة بغداد، والذي بلغ 12.8%. أظهرت نتائج التنبؤ أن نموذج BiLSTM المقترح يمكن أن يزيد بشكل كبير من دقة التنبؤات الجوية طويلة المدى لبغداد. أظهرت النتائج أن متوسط مربع الخطأ 0.53 ومعامل الارتباط 0.84 بين LST المتوقع والفعلي مما يدل على دقة جيدة. وبالتالي، يمكن استخدام النموذج المقترح لتقدير LSTs المستقبلية لبغداد مع خطأ منخفض.

1. Introduction

The measurement of LST using satellites has become an essential data source for research on modern climate change and the corresponding warming of the urban landscape. LST is closely linked to changes in the primary states of the Earth's systems, including the amounts of water vapor in the air, water in the soil, evaporation, and freezing and thawing of the land surface [1]. Furthermore, LST is an essential tool for studying the biological and physical processes occurring on the Earth's surface on both a global and regional scale. Variable changes in the Earth's surface describe the main states of the Earth's systems, which are also closely linked to LST. As a result, LST is extensively used in various academic fields, including ecology, climate research, hydrology, environmental studies, and meteorology, as well as the agricultural industry to improve crop yields [2].

Currently, three methods are used to calculate LSTs: measurements taken in the field or in situ [3], observations made by satellite [4], and model simulations. LSTs can be collected continuously using field and in situ observations, and these data are not easily impacted by the weather or other external influences. On the other hand, the utility of such data is severely limited since field stations are scattered in only a few locations [5]. The MERRA (Modern-Era Retrospective Analysis for Research and Applications) dataset from the National Center for Environmental Prediction and the ERA-Interim18 dataset are two of the most common model re-analysis datasets that can provide global LSTs that are continuous in space and time. However, the numerical models typically output these re-analysis datasets with coarse resolutions, only approximating the surface property effects on LSTs. As a result, these numerical models cannot meet the requirements of several applications, which necessitate LST data with fine resolution. Therefore, satellite remote sensing technologies are becoming increasingly widespread for the purpose of observing LSTs across the globe at appropriate temporal and spatial resolutions [6].

Several studies have successfully predicted the temperature from LST, but they face numerous challenges and limitations. Some studies utilized traditional techniques of time series analysis based on linear prediction. However, it is not very accurate, and it is essential to investigate non-linear time series techniques in order to make accurate predictions regarding LST. Machine learning techniques such as neural networks accomplish the

prediction of LST time series. Adding additional parameters can significantly influence an increase in accuracy. The introduction of new approaches and the investigation of deep learning techniques, which have recently gained popularity, have improved performance in recent years. However, there is an area to improve models by reducing the error, since even slight errors in their short-term forecasts can accumulate to become significant errors over longer periods of time. In order to address these issues, this research introduces a hybrid model that employs a bi-directional long short-term memory (BiLSTM) framework to enhance the precision of long-term LST prediction.

The remaining sections of this work are organized as follows: Section two includes a review of the related work. Section three provides a formal problem definition and background on the LSTM architecture. Section IV describes the proposed framework. Section five presents experimental data, followed by the conclusions in Section six.

2. Related Works

To recover missing data in LSTs with remotely sensed datasets, numerous techniques have been devised and implemented, and each can be categorized as a method based on the following types of information:

- Spatial [7].
- Multi-temporal [8].
- Spatiotemporal [9].

Invalid data can be recovered using cokriging interpolation algorithms, spline functions, inverse distance weighting, and pixel-disaggregating. The spatial reconstruction methods primarily use valid pixels surrounding the missing data pixel to restore the erroneous data [10]. These methods are simple to implement, functioning well in situations where the terrain is relatively uniform and the erroneous data is minimal. The main algorithms used to figure out what happened in the past are the longitudinal Fourier analysis method [15], the harmonic analysis method [11], the diurnal temperature cycle approach [13], the asymmetric Gaussian function fitting approach [14], and the temporal Fourier analysis method [11]. These techniques employ complementary temporal images for the desired regions at adjacent times to recover missing pixels. As previously noted, geostationary satellite LST data reconstruction typically uses the diurnal temperature cycle (DTC) method [16] to fully expose the diurnal shift in LSTs [17].

While these time-domain approaches are effective when filling in missing LSTs, their usefulness decreases when the number of accurate data points is insufficient to generate the model parameters. Furthermore, identifying the appropriate model to describe the DTC can be challenging, as can acquiring the optimal solution using these methods [16]. Although the results obtained from the spatial and temporal information-based methods did not meet expectations, several approaches based on spatiotemporal data for LST reconstruction have been suggested. Liu et al. [18] provided a spatiotemporal reconstruction approach for the Feng Yun-2F (FY2F) LST missing data in their work. Experiments based on simulated and real data showed that the strategy has the potential to function well, with RMSE (root mean square error) staying under roughly 2°C in the majority of the situations. In similar research, Malamiri et al. [19] provided a gap-filling strategy for LST image time-series data (TSD). Their approach used data from surrounding time periods and other more distant time periods (such as multi-year datasets or calendar dates).

However, none of these methods adequately consider spatial and temporal information concurrently. First and foremost, they require a sufficient number of data points in addition to a significant amount of human engagement. Second, if the area to be recreated is large, the procedures described above do not perform well. This is primarily because these algorithms

cannot understand the highly dynamic spatiotemporal interactions of LSTs when only a limited amount of information is available.

Convolutional neural networks (CNNs) have received increased use in the processing of remote sensing data during the past few years. They can automatically learn the inherent complicated correlations between different types of data [20]. Malek et al. [21] and Wu et al. [22] used a contextualized autoencoder CNN architecture to fix cloud-contaminated information in remote sensing images at both the pixel and patch levels. Mustafa et al. (2020) presented a model using polynomial fitting curve analysis to predict the future variation in land surface temperatures at Freetown. The study employed two land cover indices, namely MNDWI and UI, and applied a multi-regression equation to forecast future land surface temperatures (LST). The Urban Index (UI) and Modified Normalized Difference Water Index (MNDWI) accurately predicted surface temperature, with a mean relative rate percentage of 5.88% and 4.41%, respectively. The root mean square error for UI and MNDWI were 1.63 °C and 1.31 °C, respectively. The ratio of RMSE to standard deviation (RMSE/std) was 0.5 for 2010 and 0.44 for 2018. The process of urban expansion will lead to an increase in surface temperatures, particularly in the western metropolitan area of Freetown. Nimish and Bharath (2020) presented a method-based artificial neural network (ANN) and geographic technology to predict LST. The LST data from 1991 to 2000, 2009, and 2017 were used to determine the pattern and then figure out how to predict LST. The results show that as surface temperatures rise, there is a link between more concrete areas and fewer open and vegetated areas. The predicting equation that was made from the model is pretty good at making predictions. The study's results showed that ANN models can accurately predict surface temperature by taking into account a wide range of factors in a complex and changing physical world. Al-Faisal et al. (2021), Based on projected land surface temperatures (LSTs), it is expected that temperatures in the highest temperature category (over 35 °C) will rise by 13% and 20% during the summer and winter seasons, respectively, between 2020 and 2030. Every map was thoroughly analyzed to ensure accuracy and exhibited a significant level of estimation, as indicated by kappa values exceeding 80%. Ghani et al. (2021) present information for future urban planners by looking at how rising temperatures will affect the comfort of city dwellers. We used data from Landsat 7 ETM in addition to Landsat 8 OLI-TIRS to look at land cover and LST in the Kuta Selatan Sub-district over time and space for 2006, 2015, and 2020, as well as their forecasts for 2033, by employing the CA-Markov model. The findings showed that urban areas and LST increased significantly in Jimbaran, Benoa, and Tanjung Benoa in 2033. The mean LST in the Kuta Selatan Sub-district would also rise, from 25.63°C in 2006 to 33.07°C in 2033. LST is higher in built-up places and bare soil than in vegetation and bodies of water. So, plants and sources of water are very important for reducing LST. These findings show that LST in Kuta Selatan Sub-district will be warmer in the future than it is now. Similarly, in 2021, Wang et al. [23] suggested a single deep CNN to retrieve missing data in imagery from remote sensing through three different conditions (medium, high and low-spatial-resolution critical in thermal infrared (TIR) remote sensing datasets). Both approaches had good results when the missing areas were represented as neighborhoods sufficiently typical of the whole. In addition, in contrast to LST, the surface reflectance, also known as the digital number (DN), shifts subtly during the course of passing time. As a consequence, these models are not appropriate for reconstructing LSTs with a high level of spatiotemporal dynamics for vast missing sections. Ahmad et al. (2022) proposed a semi-automated classification approach to estimate land surface temperature (LST) from the years 2000 to 2020. Subsequently, the module of cellular automata-artificial neural networks (CA-ANN) was used to forecast forthcoming patterns of land surface temperature (LST) for the years 2030 and 2040, respectively. Our analysis indicates that the land surface temperature in Lahore has grown by an average of 2.8 °C over the past two decades, namely from 37.25 °C to 40.10 °C between 2000 and 2020. In addition, according to CA-ANN models, the land

surface temperature is expected to rise by 2.2 °C by 2040. By that time, the average land surface temperature is forecast to climb from 40.1 °C to 42.31 °C. The CA-ANN model was verified for future land surface temperature (LST) simulations. The validation resulted in an overall Kappa value of 0.82 and an accuracy rate of 86.2% for the years 2030 and 2040. The model used modules to evaluate land-use change. The study further suggests that land surface temperature plays a crucial role in driving environmental change. Li and Zheng (2023) introduced a technology that can forecast urban development plans and generate related heat maps of land surface temperature (LST). They have successfully developed and evaluated a Generative Adversarial Network (GAN) to anticipate city plans and the related LST heat maps. They selected New York City as a case study, utilizing light detection in addition to ranging (LiDAR) data, land surface temperature data, and other pertinent data to construct a training set of seven hundred image pairs. This training set was then used to train the model for predicting the distribution of land surface temperature (LST). By using untrained pairings and the test set, the approach is capable of rapidly and precisely generating LST maps when provided with city designs as input. Following the accuracy analysis, various scenarios are simulated to evaluate the model's ability to forecast the environmental effects of plan adjustments on land surface temperature. The scenario simulation showcases the possibilities of using this model to provide valuable insights to environmental designers regarding their detailed work.

3. Study Region and Data

3.1. Study Region

This study focuses on Baghdad, the capital and largest city of Iraq. It is situated in the middle of Iraq between 33° 18' 46.0980" North and 44° 21' 41.3568" East (Figure 1A). The study area encompasses roughly 5098 km² (Figure 1B) [24], with an average elevation of 32.1 meters above sea level. The climate of Baghdad is a semiarid and subtropical desert characterized by warm summers and cold winters [25], [26].

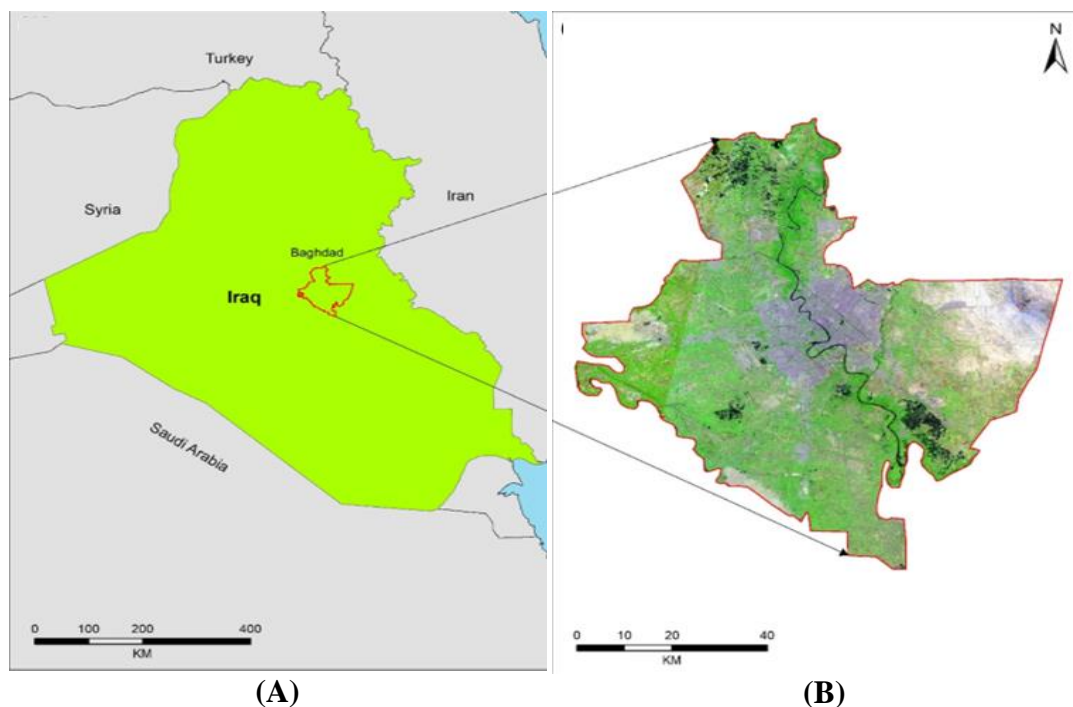


Figure 1: (A) Study area within Iraq's national border, where the red outline indicates the study area's boundary within Baghdad, and (B) a satellite image's base map [24]

3.2. Data

Data were collected from the Landsat satellites, which include Landsat 8 and Thematic Mapper, at the site of the United States Geological Survey. These photos from 1984–2018 were obtained for July and August (through the summers of every year to eliminate seasonal bias between research years) over the study area. The spatial resolution is 100 m to 30 mm [27].

4. Methodology

4.1 Dataset

The Landsat set of satellites has consistently produced space-based remote sensing data with modest resolution for over forty years. Starting on July 23, 1972, a total of 8 series of Landsat satellites have been launched specifically for the purpose of Earth Observation (EO). Landsat 6 had been the sole satellite that did not successfully attain orbit. Over the past forty years, the remaining satellites have been a valuable asset for studying and applying world change in several fields, such as agriculture, cartography, geophysics, forestry, planning for the region, surveillance, and education. For the purpose of retrieving land surface temperature (LST), a total of fifteen pictures from each Landsat series (5, 7, and 8) were used in this investigation. The Landsat data acquisition spans from 2000 until 2019, and only photos taken under clear-sky conditions were taken into account. The chosen dates guarantee the availability of in-situ data and an equal number of photos for all three Landsat missions. Landsat data is available for free download from the USGS 'Earth Explorer' website.

With a spatial resolution of 30 meters, Landsat 5 TM and Landsat 7 ETM+ feature six reflective bands, including visible, near-IR, and short-wavelength infrared. Additionally, they have one band in the thermal infrared (TIR) area, specifically Band 6. The thermal band has an inherent spatial resolution of 120 meters and 60 meters for TM and ETM+ sensors, respectively. However, the USGS achieves a higher resolution of 30 m by applying cubic convolution resampling. The Landsat 8 OLI sensor consists of nine reflecting bands that provide a spatial resolution of 30 meters. Additionally, the Landsat 8 TIRS sensor includes two bands specifically designed for thermal infrared radiation, known as Band 10 and Band 11. The USGS resampled and released the thermal bands at a higher resolution of 30 meters, despite their original natural spatial resolution of 100 meters.

4.2. LST Forecasting Method

The normalized difference vegetation index N_{DVI} can be derived from the spectral reflectance of Landsat imagery [28] [29]:

$$N_{DVI} = \frac{(N_{IR} - R_r)}{(N_{IR} + R_r)}, \quad (1)$$

where N_{IR} is the near-infrared (N-IR) spectral reflectance, where the reflectance being at the top of the canopy is most prominent, and R_r is the reflectance in the red section of the spectrum, where chlorophyll absorbs a significant amount of light.

The normalized difference built-up index N_{DBI} can be derived from the shortwave-infrared (SW-IR) spectral reflectance [30]:

$$N_{DBI} = \frac{(S_{IR} - R_r)}{(S_{IR} + R_r)}, \quad (2)$$

where the properties of spectral reflectance from the N-IR toward the SW-IR make differentiating between the built-up areas and the desolate land and other aspects of the terrain possible. The values of N_{DBI} range from -1 to $+1$, with 0 representing woodland and agriculture, -1 representing water bodies, and $+1$ representing built-up pixel coverage in the

research region. The built-up regions quantified from the NDBI pictures were utilized in this study to evaluate the impact urbanization has on the spatial variability of LST in the area of the study.

The data from Landsat were changed such that they correspond to the spectral radiance of the top-of-atmosphere (TOA) L_λ ($\text{W}/(\text{m}^2 \cdot \text{srad} \cdot \mu\text{m})$), defined as [31]:

$$L_\lambda = M_L Q_{cal} + A_L, \quad (3)$$

where Q_{cal} is the pixel DN and M_L and A_L represent band-specific multiplicative and additive rescaling factors, respectively.

Brightness temperature (TB) in Kelvin is a measurement of thermal radiation that moves vertically toward a satellite from the TOA [32]:

$$TB = \frac{K_1}{\ln\left(\frac{K_2}{L_\lambda} + 1\right)}, \quad (4)$$

where K_1 and K_2 are constants (W/m).

The temperature is then converted to Celsius by subtracting 273.15 from the original reading [32], [33]:

$$T_B = \frac{K_2}{\ln\left(\frac{K_2}{L_\lambda} + 1\right)} - 273.15, \quad (5)$$

The LST maps in years 1985, 2001, and 2018 are derived from Landsat 5 and 8 images in a respective year and can be calculated from:

$$LST = \frac{T_B}{1 + (\lambda(T_B) \times \ln(\varepsilon/\rho))}, \quad (6)$$

where LST is in units of Celsius, T_B is the brightness temperature at-sensor ($^\circ\text{C}$), ε is the emissivity of the land surface, and λ ($11.5 \mu\text{m}$) is the wavelength of the emitted radiance ρ , which is equal to the following:

$$\rho = P \frac{c}{\delta} = 1.438 \times 10^{-2} \text{ m} \cdot \text{K}, \quad (7)$$

where P is Planck's constant, δ is the Stefan-Boltzmann constant, and c is the light velocity.

4.3. Classification

This section divides the study area into zones that share similar LST characteristics. To forecast the LSTs for the time steps, a long short-term memory (LSTM)-based deep neural network is used. Figure 2 shows the LSTM architecture. The study can utilize LSTM as an acute model of deep learning due to its impressive learning potential. The benefit of using LSTM is that it can solve fading error backflow because of its default behaviors in capturing long-term dependence, and it prevents the practical loss of tiny time lags.

Allow sequence data in the notation $x = (x_1, x_2, x_3, \dots, x_t)$ as an input to estimate the output state using $h = (h_1, h_2, h_3, \dots, h_t)$ and cell state $c = (c_1, c_2, c_3, \dots, c_t)$, respectively. The initial value in a sequence x (x_1) is implemented in the first LSTM unit, resulting in the initial value of the updated cell state c_1 and the hidden state h_1 .

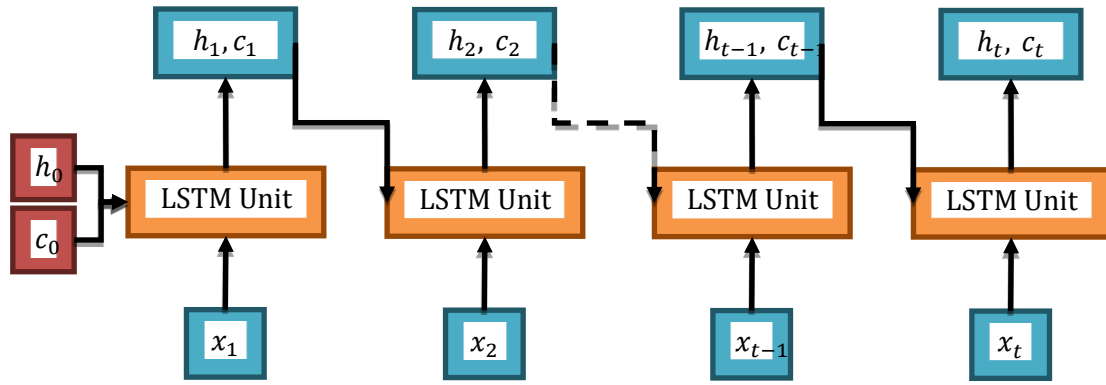


Figure 2: LSTM architecture

From time step t , the input vector x_t and output vector of the previous step h_{t-1} pass through the memory cells. After adjusting the three gates, the LSTM outputs h_t and updates the cell state c_t . The terms W_f , W_c , W_i , and W_o are weight matrices in the Equations (8–10, 12).

At time step t , the memory cells are exposed to the input vector x_t and the output vector h_{t-1} . The LSTM changes the cell state once the three gates are adjusted and then produces h_t , using the following steps:

1. The LSTM network ascertains the specific information to be discarded from the preceding cell state, denoted as c_{t-1} . The forget gate unit calculates the input vector x_t and the outputs h_{t-1} of the memory cells from the previous step, along with the forget gate bias b_f [34]:

$$f_t = \text{sigmoid}(W_f[x_t, h_{t-1}] + b_f), \quad (8)$$

The range of the function f_t is adjusted by the application of the sigmoid function σ , which restricts the output values between 0 (indicating total removal) and 1 (indicating complete retention).

2. The LSTM model ascertains the content to be stored as new information within the cell state, denoted as c_t . This involves the incorporation of an additional candidate value \hat{c}_t into the cell state, as well as the process of updating information within the cell state [34]:

$$\hat{c}_t = \tanh(W_c[x_t, h_{t-1}] + b_c), \quad (9)$$

$$i_t = \sigma(W_i[x_t, h_{t-1}] + b_i), \quad (10)$$

3. The cell state is updated using the output values obtained from the previous stage:

$$c_t = f_t c_{t-1} + i_t \hat{c}_t, \quad (11)$$

4. The LSTM model determines the output h_t :

$$o_t = \sigma(W_o[x_t, h_{t-1}] + b_o), \quad (12)$$

$$h_t = o_t \tanh(c_t), \quad (13)$$

In addition to LSTM, the activation function type (leaky ReLUs) is utilized, and the regularization of dropouts is introduced to minimize overfitting. Both of these features are applied in conjunction with dropout regularization. As a candidate for the optimization function, the adaptive moment estimate is selected. Many different hyperparameters are involved in the learning process associated with deep neural networks, involving several factors such as training iterations, momentum, dropout ratio, initial learning rate, the number of layers, the number of hidden neurons, and the learning rate schedule.

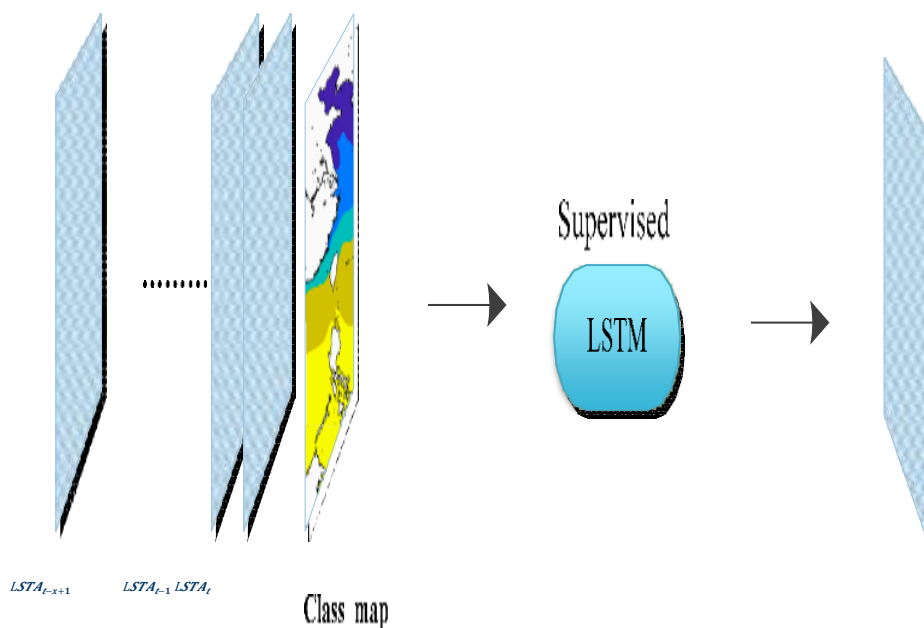


Figure 3: Proposed LSTM model

In this research, we present a bi-directional LSTM (BiLSTM) model to overcome the individual shortcomings of LSTM and take full advantage of its respective features. Figure 4 displays the typical BiLSTM architecture. We created our BiLSTM model specifically using BiLSTM layers. This model consists of nine layers. Every other layer is a dropout layer, and to prevent the model from becoming overly specific, the model removes 20% of the random nodes from the layer below. It has three additional layers of simple LSTM on top of the one layer of BiLSTM it has. We start our model with the first layer of BiLSTM, add three layers of BiLSTM, and then insert dropout layers between each stage.

The problem of overfitting occurs when a model's parameters become excessively fixed based on the training set and the validation datasets. The model performs extremely well on the training datasets, but not as well on the test datasets or in predicting. To address this issue, we include dropout layers after each successive layer.

Cross-validation, feature selection, and regularization are a few of the potential alternatives that may help circumvent the overfitting phenomenon. Because we train data for several types by partitioning them into portions, cross-validation is computationally intensive and time-consuming. When a limited number of training samples are available but a large number of features are available, the feature selection approach should be used. To prevent the model from becoming overly specific, only the most critical features are chosen for its training using feature selection methods, such as computing the correlation coefficient and selecting K_{Best} .

The process of adding a penalty to the error function is referred to as regularization, which allows the coefficients to be modified in a way that prevents the predictions from taking on excessively high or low values. In this particular scenario, we use dropout layer approaches because the number of features is insufficient for the feature selection method to be useful, and cross-validation requires significant processing resources. Regularization is not helpful, as we have already removed the outliers. Therefore, even if we do not utilize these procedures, the outcomes remain relatively unchanged.

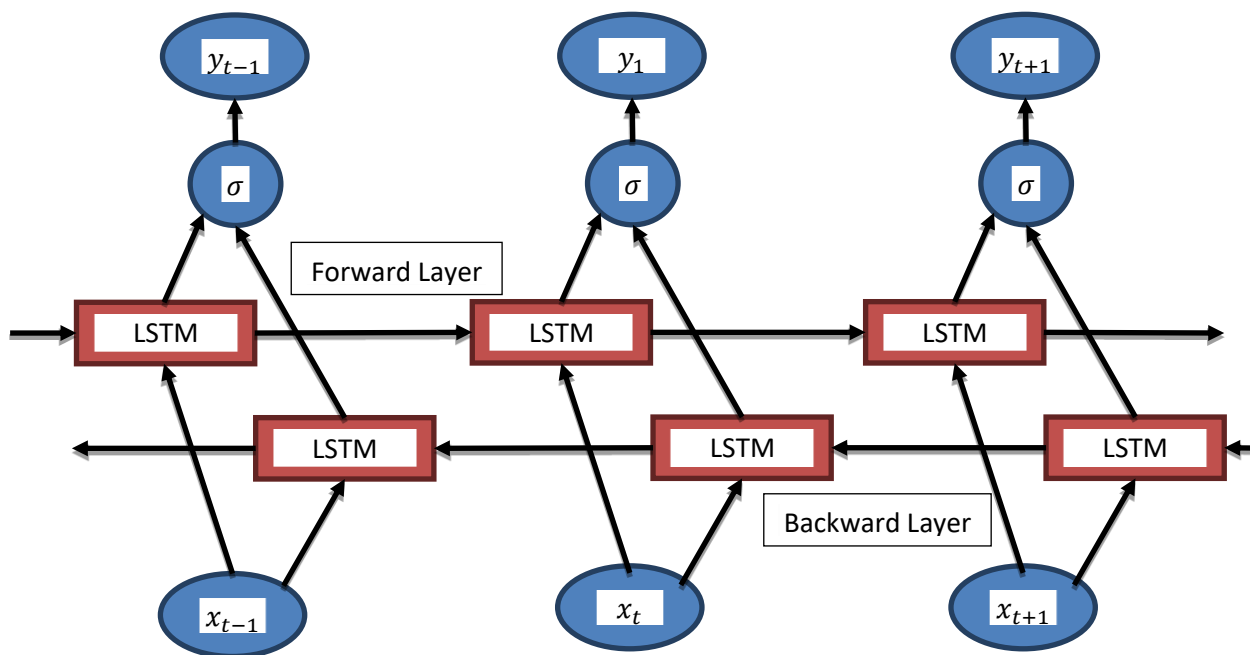


Figure 4: Typical BiLSTM architecture

5. Results and Discussion

5.1. Historical LST Analysis

First, we analyzed both predicted and actual LST values of satellite images using our proposed color segment and percentage calculations, as shown in Figure 5.

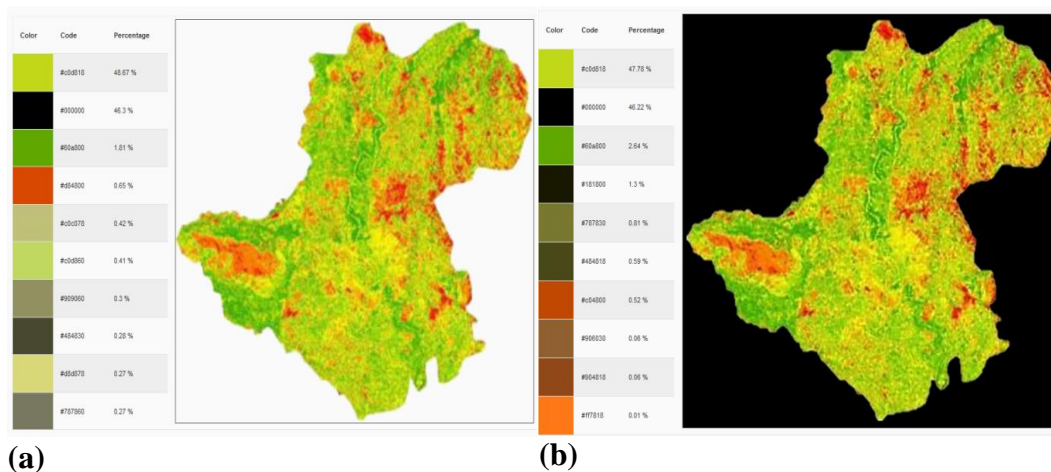


Figure 5: LST color variation analysis for Baghdad for 1984. (a) Actual LST and (b) predicted LST [27]

From Figure 5, both images are similar, where we extracted the area (in black/white) outside the Baghdad border, which is about 46.3% of the total image. Using the mean-squared error (MSE) as well as the correlation coefficient R , we can assess the qualitative and quantitative accuracy of the calculated LST plot in relation to the observation. The spread of plans seen in 1984 and those predicted for 2018 exhibit very good agreement. In 2018, the mean error is small, while the R and MSE between the predicted and actual LST are 0.84 and 0.53, respectively, showing a significant correlation between the two. Figure 6 shows the estimated LSTs for 1984, 2001, and 2018, together with the predicted LSTs for 2030–2050.

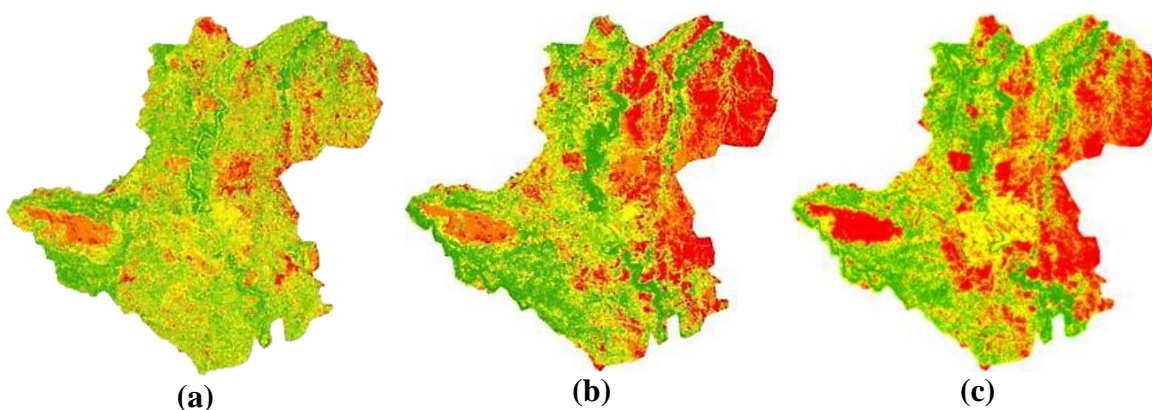


Figure 6: LST variation in Baghdad for three periods of time: (a) 1984, (b) 2001, and (c) 2018 [27]

LST patterns were forecasted using three separate Landsat scenes from the corresponding years. The Figure 6 color scheme represents the temperature gradient from colder to warmer conditions in the research area, with green and red indicating lower and higher temperatures, respectively.

Based on the data, it appears that the northeast (NE) and southeast (SE) have experienced the greatest temperature rises from 2001 to 2018. In 1984, the low temperature covered about 90% of the Baghdad area, in which the LST zones were <15°C covered 22.1%, <20°C covered 15.5%, <25°C covered 23.4%, <35°C covered 25.8%, and >35°C covered the smallest area. In 2018, a fast-staggering LST occurred at >35°C due to the net change in the Baghdad area, which was 12.8% over the previous year, 2001, as presented in Table 1 and Figure 7.

Table 1: LST distribution (% area of Baghdad) for 1984, 2001, and 2018 [27]

LST Year	<15°C	<20°C	<25°C	<35°C	>35°C
1984	22.1	15.5	23.4	25.8	13.2
2001	19.3	6.9	18.3	26	29.5
2022	7.5	6.4	14.9	28.9	42.3

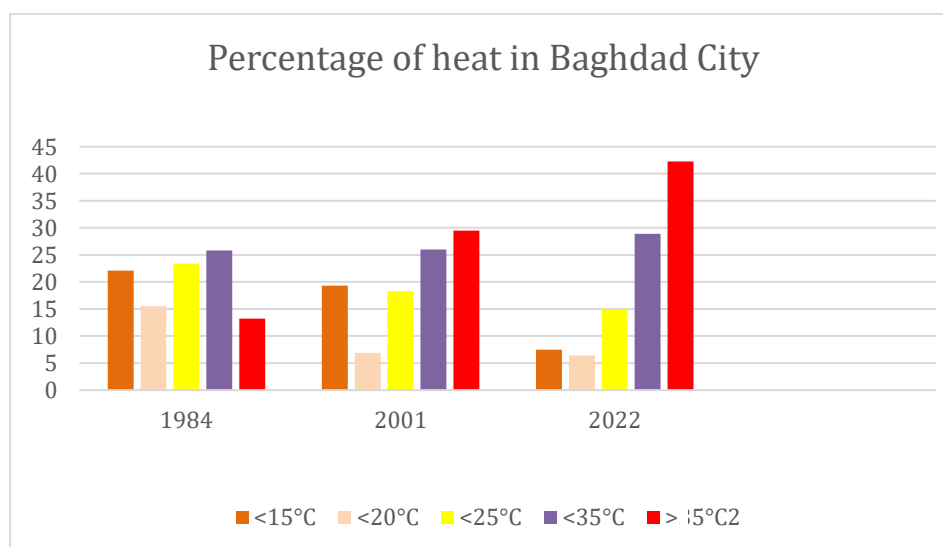


Figure 7: Distribution of LST in Baghdad in 1984, 2001, and 2018 [27]

5.2. Analysis of Predicted LST for Future

The predicted LST of Baghdad changes significantly from 2030 to 2050, as shown in Figure 8.

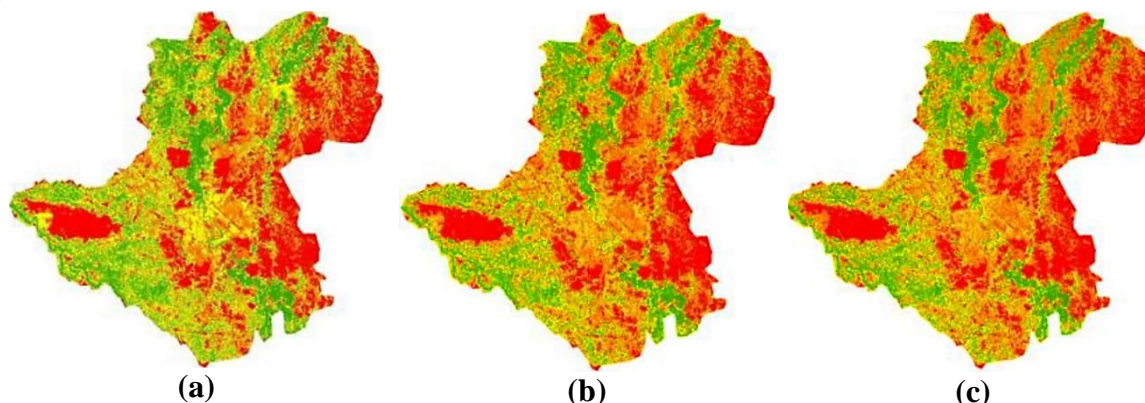


Figure 8: Predicted LST for Baghdad: (a) 2030, (b) 2040, and (c) 2050

To detect potential implications of climate change and ecosystems in the region, accurate predictions of LST patterns are essential. By examining historical LST trends, the proposed model could provide predictions for 2030, 2040, and 2250. Figure 9 and Table 2 display the prediction results.

Table 2: Expected LST distribution (% area of Baghdad) for 2030, 2040, and 2050

LST Years	<25°C	<30°C	<35°C	<40°C	>40°C
2030	20.4	10.1	16	15.3	38.2
2040	17.3	9.8	16.7	16.5	39.7
2050	7.5	6.4	22.4	11.8	48.1

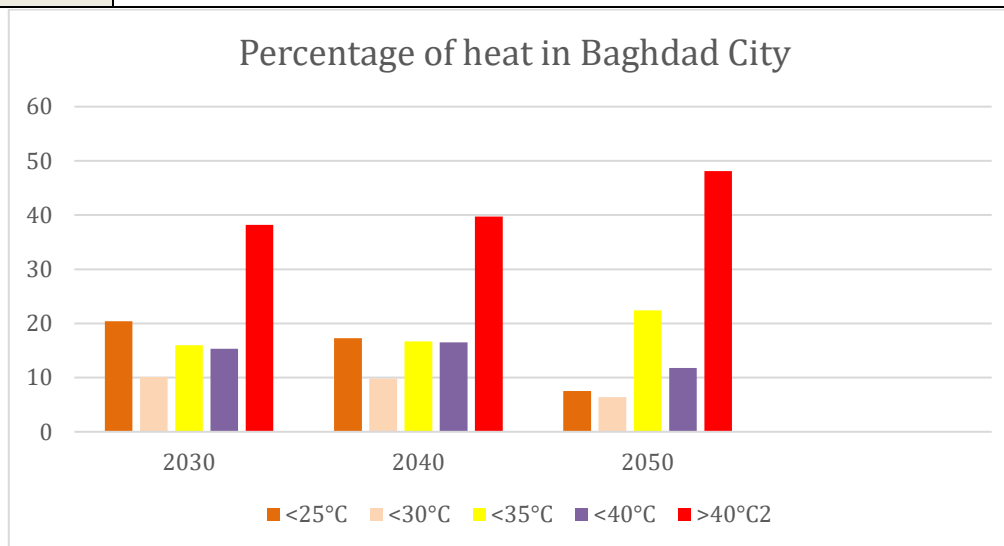


Figure 9: Distribution degree of LST in Baghdad from 2030 to 2050

From Figure 9 and Table 2, we determine that the average LST of Baghdad from 2030 to 2050 ranges from 25°C to 48°C, indicating that the average LST in the future will be higher than in the past by 2.83°C.

6. Conclusion

The precise estimation of LST is critical in thermal infrared (TIR) remote sensing. Based on the thermal radiance transmission equation, the results recorded in each channel are influenced by emissivity, atmospheric factors, and LST. The present study employed the BiLSTM model to forecast LST by including LST data from preceding years and elevation input parameters into the LSTM model. When compared to other gold-standard models, our A deep learning model-based Bi-LSTM model shows promising validation results. The MSE and the correlation coefficient R between the predicted and actual LST of 0.84 and 0.53, respectively, indicate good accuracy and a significant correlation between the observed and the anticipated LST. The prediction results for the average LST of Baghdad from 2030 to 2050 show a range from 25°C to 48°C, indicating that the average LST in the future will be higher than 20 years prior by 2.83°C. Through an application-based deep learning approach, our research on LST prediction can inform government authorities and urban planners in Iraq to take protective measures for the country's natural resources. In the future, we hope to classify hyperspectral data using real-time scenarios and use the bands from hyperspectral data to derive the temperature levels associated with each pixel.

References

- [1] Sajjad Hussain, Ali Raza, Hazem Ghassan Abdo, Muhammad Mubeen, Aqil Tariq, Wajid Nasim, Muhammad Majeed, Hussein Almohamad, and Ahmed Abdullah Al Dughairi, "Relation of land surface temperature with different vegetation indices using multi-temporal remote sensing data in Sahiwal region, Pakistan," *Geoscience Letters*, vol. 10, pp. 1-15, 2023.
- [2] Glynn C. Hulley, Darren Ghent, Frank M. Göttsche, Pierre C. Guillevic, David J. Mildrexler, and César Coll, "Land Surface Temperature," *Taking the Temperature of the Earth*, Elsevier, pp. 57–127, Jan. 2019, Doi: 10.1016/B978-0-12-814458-9.00003-4
- [3] Praveena Krishnan, Tilden P. Meyers, Simon J. Hook, Mark Heuer, and David Senn, "Intercomparison of In Situ Sensors for Ground-Based Land Surface Temperature Measurements," *Sensors*, vol. 20, no. 18, pp. 5268-5293, 2020.
- [4] Zhao-Liang Li, Hua Wu, Si-Bo Duan, Wei Zhao, Huazhong Ren, Xiangyang Liu, Pei Leng, Ronglin Tang, Xin Ye, Jinshun Zhu, Yingwei Sun, Menglin Si, Meng Liu, Jiahao Li, Xia Zhang, Guofei Shang, Bo-Hui Tang, Guangjian Yan, and Chenghu Zhou, "Satellite remote sensing of global land surface temperature: Definition, methods, products, and applications," *Reviews of Geophysics*, vol. 61, no. 1, pp. 1-77, 2023.
- [5] Aliihsan Sekertekin, and Elaheh Zadbagher, "Simulation of future land surface temperature distribution and evaluating surface urban heat island based on impervious surface area," *Ecological Indicators*, vol. 122, no. 1, pp. 1-12, 2021.
- [6] Pei Yu, Tianjie Zhao, Jiancheng Shi, Youhua Ran, Li Jia, Dabin Ji, and Huazhu Xue, "Global spatiotemporally continuous MODIS land surface temperature dataset," *Scientific Data*, vol. 9, pp. 1-15, 2022.
- [7] Christian Berger, J. Rosentreter, M. Voltersen, C. Baumgart, C. Schmullius, and S. Hese, "Spatio-temporal analysis of the relationship between 2D/3D urban site characteristics and land surface temperature," *Remote Sens Environment*, vol. 193, pp. 225-243, 2017.
- [8] Tommaso Barbieri, Despina Francesca, and Teggi Sergio, "A Multi-Temporal Analyses of Land Surface Temperature Using Landsat-8 Data and Open Source Software: The Case Study of Modena, Italy," *Sustainability*, vol. 10, no. 5, pp. 1-13, 2018.
- [9] Xinyan Hou, Xie Xuan, Bagan Hasi, Chen Chaomin, Wang Qinxue, and Yoshida Takahiro, "Exploring Spatiotemporal Variations in Land Surface Temperature Based on Local Climate Zones in Shanghai from 2008 to 2020," *Remote Sensing*, vol. 15, no. 12, pp. 1-17, 2023.
- [10] S. Hsua, A. Mavrogiannib, and I. Hamiltona, "Comparing Spatial Interpolation Techniques of Local Urban Temperature for Heat-related Health Risk Estimation in a Subtropical City," *Procedia Engineering*, vol. 198, pp. 354-365, 2017.
- [11] Jorn P. Scharlemann, David Benz, Simon I. Hay, Bethan V. Purse, Andrew J. Tatem, G. R.

- Wint, and David J. Rogers, "Global data for ecology and epidemiology: A novel algorithm for temporal Fourier processing MODIS data," *PloS one*, vol. 3, no. 1, pp. 1-20, 2008.
- [12] Yongming Xu, and Yan Shen, "Reconstruction of the land surface temperature time series using harmonic analysis," *Computers & Geosciences*, vol. 61, pp. 126-132, 2013.
- [13] Si-Bo Duan, Zhao-Liang Li, Bo-Hui Tang, Hua Wu, Ronglin Tang, Yuyun Bi, and Guoqing Zhou, "Estimation of Diurnal Cycle of Land Surface Temperature at High Temporal and Spatial Resolution from Clear-Sky MODIS Data," *Remote Sensing*, vol. 6, no. 4, pp. 3247-3262, 2014.
- [14] Qiang Xiao, Jianping Tao, Yang Xiao, and Feng Qian, "Monitoring vegetation cover in Chongqing between 2001 and 2010 using remote sensing data," *Environmental Monitoring and Assessment*, vol. 189, no. 10, pp. 899-915, 2017.
- [15] Reiners Philipp, José Sobrino, and Claudia Kuenzer, "Satellite-Derived Land Surface Temperature Dynamics in the Context of Global Change—A Review," *Remote Sensing*, vol. 15, no. 7, pp. 1857-1889, 2023.
- [16] Si-Bo Duan, Zhao-Liang Li, Bo-Hui Tang, Hua Wu, and Ronglin Tang, "Direct estimation of land-surface diurnal temperature cycle model parameters from MSG–SEVIRI brightness temperatures under clear sky conditions," *Remote Sensing of Environment*, vol. 150, pp. 34-43, 2014.
- [17] Guillermo Federico Olmedo, Samuel Ortega-Farías, Daniel de la Fuente-Sáiz, David Fonseca Luego, and Fernando Fuentes-Peñailillo, "water: Tools and Functions to Estimate Actual Evapotranspiration Using Land Surface Energy Balance Models in R Introduction and motivation," *The R Journal*, vol. 8, no. 2, pp. 352-369, 2016.
- [18] Z. Liu, P. Wu, S. Duan, W. Zhan, X. Ma and Y. Wu, "Spatiotemporal Reconstruction of Land Surface Temperature Derived from FengYun Geostationary Satellite Data," *IEEE Journal of Selected Topics in Applied Earth Observations and Remote Sensing*, vol. 10, no. 10, pp. 4531-4543, 2017.
- [19] H. R. G. Malamiri, I. Rousta, H. Olafsson, H. Zare, and H. Zhang, "Gap-Filling of MODIS Time Series Land Surface Temperature (LST) Products Using Singular Spectrum Analysis (SSA)," *Atmosphere*, vol. 9, no. 9, pp. 1-118, 2018.
- [20] Binh Minh Nguyen, Ganglin Tian, Minh-Triet Vo, Aur'elie Michely, Thomas Corpettiz, Carlos and Granero-Belinchon, "Convolutional Neural Network Modelling for MODIS Land Surface Temperature Super-Resolution," 2022 30th European Signal Processing Conference (EUSIPCO), Belgrade, Serbia, 2022, pp. 1806-1810, doi: 10.23919/EUSIPCO55093.2022.9909569.
- [21] Salim Malek, Farid Melgani, Yaqoub Bazi, and Niaf Alajlan, "Reconstructing cloud-contaminated multispectral images with contextualized autoencoder neural networks," *IEEE Transactions on Geoscience and Remote Sensing*, vol. 56, no. 4, pp. 2270-2282, 2018.
- [22] Penghai Wu, Zhixiang Yin, Hui Yang, Yanlan Wu, and Xiaoshuang Ma, "Reconstructing Geostationary Satellite Land Surface Temperature Imagery Based on a Multiscale Feature Connected Convolutional Neural Network," *Remote Sensing*, vol. 11, no. 3, pp. 1-18, 2019.
- [23] Han Wang, Kebiao Mao, Zijin Yuan, Jiancheng Shi, Mengmeng Cao, Zhihao Qin, Sibao Duan, and Bohui Tang, "A method for land surface temperature retrieval based on model-data-knowledge-driven and deep learning," *Remote Sensing of Environment*, vol. 265, pp. 1-19, 2021.
- [24] Shahad Mohammed Ahmed, and Fouad K. Mashee Al-Ramahi, "Evaluate the Effect of Relative Humidity in the Atmosphere of Baghdad City urban expansion Using Remote Sensing Data," *Iraqi Journal of Science*, vol. 63, no. 4, pp. 1848-1859, 2022.
- [25] Ali K. Mohammed Ali, and Fouad K. Mashee Al Ramahi, "A study of the Effect of Urbanization on Annual Evaporation Rates in Baghdad City Using Remote Sensing," *Iraqi Journal of Science*, vol. 61, no. 8, pp. 2142-2149, 2020.
- [26] Ghufraan Ameer, and Nawal Kh. Gazal, "Determining the features on the image of Satellite Sentinel-2 with different resolution and comparing them with images of Satellite Sentinel-1," *Journal of Physics: Conference Series*, pp. 2114-2137, 2021.
- [27] U. s. f. a. c. world, "Landsat 8 | U.S. Geological Survey," [Online]. Available: <https://www.usgs.gov/landsat-missions/landsat-8>.

- [28] A. S. M. Abdul Athick, K. Shankar, and H. R. Naqvi, "Data on time series analysis of land surface temperature variation in response to vegetation indices in twelve Wereda of Ethiopia using mono window, split window algorithm and spectral radiance model," *Data in Brief*, vol. 27, pp. 1-12, 2019.
- [29] A. S. Mahdi, "The Land Use and Land Cover Classification on the Urban Area," *Iraqi Journal of Science*, vol. 63, no. 10, pp. 4609-4619, 2022.
- [30] Komal Gadekar, Chaitanya B. Pande, J. Rajesh, S. D. Gorantiwar, and A. A. Atre, "Estimation of Land Surface Temperature and Urban Heat Island by Using Google Earth Engine and Remote Sensing Data," in *Springer Climate*, Springer, Cham, 2023, pp. 367-389.
- [31] Yaw A. Twumasi, Edmund C. Merem, John B. Namwamba, Olipa S. Mwakimi, Tomas Ayala-Silva, Diana B. Frimpong, Zhu H. Ning, Abena B. Asare-Ansah, Jacob B. Annan, Judith Oppong, Priscilla M. Loh, and Faustina Owusu., "Estimation of Land Surface Temperature from Landsat-8 OLI Thermal Infrared Satellite Data. A Comparative Analysis of Two Cities in Ghana," *Advances in Remote Sensing*, vol. 10, no. 4, pp. 131-149, 2021.
- [32] Mitiku Badasa Moisa, Bacha Temesgen Gabissa, Lachisa Busha Hinkosa, Indale Niguse Dejene, and Dessalegn Obsi Gemedo, "Analysis of land surface temperature using Geospatial technologies in Gida Kiremu, Limu, and Amuru District, Western Ethiopia," *Artificial Intelligence in Agriculture*, vol. 6, pp. 90-99, 2022.
- [33] Ahmed F. Hassoon, and Abdulrahman B. Ali, "Irregular urban Expansion and Its Effects on Air Temperature over Baghdad City using Remote Sensing Technique," *Iraqi Journal of Science*, vol. 62, no. 6, pp. 2110-2121, 2021.
- [34] Sida Xing, Feihu Han, and Dr Sui Yang Khoo, "Extreme-Long-short Term Memory for Time-series Prediction," *arXiv:2210.08244*, pp. 1-19, 2022.